Bang-Bang Control of Electro-hydraulic Servomechanisms

By

Hideo HANAFUSA* and Keiichiro MIYATA*

(Received April 17, 1969)

The optimum control is given for an electro-hydraulic servomechanism. It is approximated by two quasi-optimum controls which are reasonable in point of the control sensitivity and the practical construction of control system.

The optimum control is obtained by the bang-bang control except in a very special case. The optimum switching points are determined as intersections of the phase trajectories and the switching surface in the phase space. We determine the switching points by the projections on the phase plane.

The switching based on the fixed mathematical model is not favorable for considering the sensitivities to parameter variations.

Two quasi-optimum controls are considered. One is obtained by approximating the optimum switching curve by two lines on the phase plane, the other by approximating the switching surface by a switching plane in the phase space. The errors due to the approximations are investigated.

The satisfactory results are obtained in experiments and the advantages of this method are verified.

1. Introduction

Electro-hydraulic servomechanisms have high performance in point of the response speed and the control accuracy, but the compressibility of oil and the friction of the actuator sometimes prevent obtaining the required accuracy when the conventional feedback control systems are used.

Now, we provide a practical method to realize the simple and accurate control. System equations contain the effect of the friction of the actuator.[1] The time optimum control is obtained from Pontryagin's maximum principle.[2] The sensitivities[3] to the system parameters are discussed.

Two kinds of quasi-optimum controls[4] are presented. One is a conventional position-plus-velocity feedback control. The other is a quasi optimization method with an acceleration feedback in addition to the above two feedbacks. The experiments of the actual equipments verified the validity and advantages of this method.

* Automation Research Laboratory

2. State Equations of the Hydraulic Driving System

The block diagram of the servo system is shown in Fig. 1. Considering the compressibility of hydraulic oil and the frictions of the actuator, the equation of motion of the valve-cylinder system enclosed by brocken lines is written with a non-dimensional expression, Eq. (1).

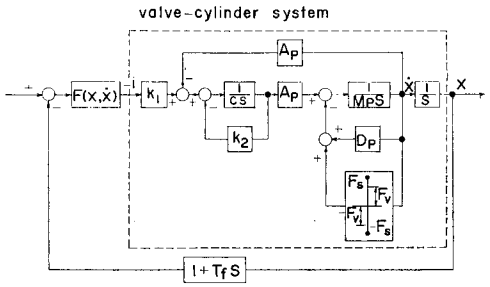

Fig. 1. Block diagram of a valve-controlled electro-hydraulic servomechanism

$$\frac{d^3z}{d\tau^3}+2\zeta\frac{d^2z}{d\tau^2}+\frac{dz}{d\tau}=-(u-q)\,,\quad |u|\leq 1\,, \tag{1}$$

where

$$z=x/(I_m/\omega_n)\,,\quad \omega_n^2=(A_p^2+k_2D_p)/CM_p\,,$$
$$u=I/I_m\,,\quad I=k_1A_pi/(A_p^2+k_2D_p)\,,\quad q=k_2F_v/k_1A_pi_m\,,$$
$$\tau=\omega_nt\,,\quad \zeta=(CD_p+M_pk_2)/2\{CM_p(A_p^2+k_2D_p)^{1/2}\}\,.$$

Eq. (1) is written with state variables as follows;

$$\dot{\boldsymbol{Z}}=\boldsymbol{MZ}+\boldsymbol{N}\,, \tag{2}$$

where $\cdot$ means the differentiation by τ, and

$$z=z_1\,,\quad \boldsymbol{Z}=\begin{pmatrix}z_1\\z_2\\z_3\end{pmatrix},\quad \boldsymbol{M}=\begin{pmatrix}0&1&0\\0&0&1\\0&-1&-2\end{pmatrix},\quad \boldsymbol{N}=\begin{pmatrix}0\\0\\-u+q\end{pmatrix}.$$

The problem is that the load should be tpansported from $x=x_0$ to $x=0$. Initial and terminal conditions are

$$\boldsymbol{Z}_0=\begin{pmatrix}x_0/(I_m/\omega_n)\\0\\-(F_s-F_v)/M_p\omega_nI_m\end{pmatrix}\equiv\begin{pmatrix}A\\0\\-B\end{pmatrix} \tag{3}$$

$$\boldsymbol{Z}_T = \begin{pmatrix} 0 \\ 0 \\ P \end{pmatrix} \tag{4}$$

$\tau=0$ and $\tau=T$ indicate the time of the beginning and the end of the motion, respectively. If the inertia force is less than the static friction force, the system stops at the terminal. This condition is

$$0<P<(F_s+F_v)\,C^{1/2}/M_p^{1/2}(A_p^2+k_2D_p)^{1/2}\,I_m\,, \tag{5}$$

where P represents the acceleration at the terminal.

3. Optimal Control

3.1 Time Optimum Control of the System with $\zeta \geq 1$

When $\zeta \geq 1$, the characteristic equation of Eq. (1) has real roots and the response of the system is non-oscillatory. The optimum control for $\zeta \geq 1$ is obtained by Pontryagin's maximum principle. The roots of the characteristic equation of Eq. (1), λ_1, λ_2 and λ_3 are

$$\lambda_1 = -\zeta+(\zeta^2-1)^{1/2}\,, \quad \lambda_2 = -\zeta-(\zeta^2-1)^{1/2} \text{ and } \lambda_3 = 0\,. \tag{6}$$

Then, Eq. (2) is transformed to a canonical form[5] as

$$\frac{d\boldsymbol{Y}}{d\tau} = \boldsymbol{K}\boldsymbol{Y}+\boldsymbol{L}(u-q) \tag{7}$$

where

$$\boldsymbol{Y} = \begin{pmatrix} y_1 \\ y_2 \\ y_3 \end{pmatrix} = \begin{pmatrix} \lambda_2 z_2 - z_3 \\ \lambda_1 z_1 - z_3 \\ -z_1+(\lambda_1+\lambda_2)z_2 - z_3 \end{pmatrix}, \quad \boldsymbol{K} = \begin{pmatrix} \lambda_1 & 0 & 0 \\ 0 & \lambda_2 & 0 \\ 0 & 0 & 0 \end{pmatrix}, \quad \boldsymbol{L} = \begin{pmatrix} 1 \\ 1 \\ 1 \end{pmatrix} \tag{8}$$

The initial and terminal conditions in canonical form become

$$\begin{aligned} &y_{10} = B\,, \quad y_{20} = B \quad \text{and} \quad y_{30} = B-A\,, \quad \text{when} \quad \tau = 0\,, \\ &y_{1T} = -P\,, \quad y_{2T} = -P \quad \text{and} \quad y_{3T} = -P\,, \quad \text{when} \quad \tau = T\,. \end{aligned} \tag{9}$$

Introducing adjoint variables, ψ_1, ψ_2 and ψ_3, Hamiltonian H is constructed from Eq. (7) as follows,

$$H = -1+\psi_1\lambda_1 y_1+\psi_2\lambda_2 y_2+(u-q)(\psi_1+\psi_2+\psi_3)\,, \tag{10}$$

where

$$\frac{d\psi_1}{d\tau} = -\frac{\partial H}{\partial y_1} = -\lambda_1\psi_1$$
$$\frac{d\psi_2}{d\tau} = -\frac{\partial H}{\partial y_2} = -\lambda_2\psi_2 \tag{11}$$
$$\frac{d\psi_3}{d\tau} = -\frac{\partial H}{\partial y_3} = 0 .$$

Assuming ψ_{10}, ψ_{20} and ψ_{30} as the initial value of ψ_1, ψ_2 and ψ_3, respectively, the solutions of Eq. (11) are obtained as follows;

$$\psi_1 = \psi_{10}\, e^{-\lambda_1\tau}, \quad \psi_2 = \psi_{20}\, e^{-\lambda_2\tau} \quad \text{and} \quad \psi_3 = \psi_{30} .$$

Hamiltonian H should be maximum at any τ according to the maximum principle. This means

$$u = \operatorname{sgn}(\psi_1+\psi_2+\psi_3) = \operatorname{sgn}\{g(\tau)\}, \tag{12}$$

where

$$g(\tau) = \psi_{10}\, e^{-\lambda_1\tau}+\psi_{20}\, e^{-\lambda_2\tau}+\psi_{30}, \qquad |u| \leq 1 .$$

From the transversality condition at the terminal,

$$\psi_{1T}+\psi_{2T}+\psi_{3T} = 0 . \tag{13}$$

Obviously, $u=1$ should be used at the beginning and it means

$$\psi_{10}+\psi_{20}+\psi_{30} > 0 . \tag{14}$$

The sign of $g(\tau)$ changes two times at most, because ψ_1 and ψ_2 change exponentially and ψ_3 is constant. As the value of $g(\tau)$ at $\tau=T$ is zero by Eq. (13), $g(\tau)$ becomes zero only once during the control process. This means

$$\psi_{10}<0, \quad \psi_{20}>0 \quad \text{and} \quad \psi_{30}>0 .$$

$g(\tau)$ changes as Fig. 2 and the optimum control can be accomplished by one switching of u.

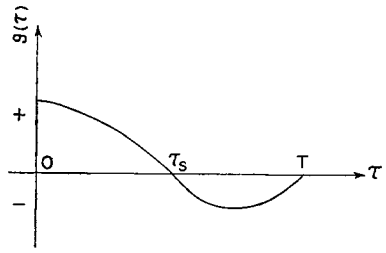

Fig. 2. Chang of $g(\tau)$ vs. τ

3.2 Optimum Switching

The optimum switching points are determined by the intersections of the forward trajectories which start from $\boldsymbol{Z}=\boldsymbol{Z}_0$ with $u=1$ and the reverse trajectories which terminate at the terminal point with $u=-1$.

From Eq. (2), the forward trajectories become

$$\boldsymbol{Z}(\tau) = \boldsymbol{\phi}(\tau)\boldsymbol{Z}_0+\int_0^{\tau}\boldsymbol{\phi}(\tau-s)\boldsymbol{N}_1 ds\,, \tag{15}$$

where $\boldsymbol{\phi}(\tau)$ is the transition matrix of Eq. (2) and

$$\boldsymbol{Z}(\bar{\tau}) = \boldsymbol{\phi}(-\bar{\tau})\boldsymbol{Z}_T+\int_0^{\bar{\tau}}\boldsymbol{\phi}(s-\bar{\tau})\boldsymbol{N}_2 ds\,, \tag{16}$$

where $\boldsymbol{\phi}(-\tau)$ is the transition matrix in the reverse time, $\bar{\tau}=T-\tau$, and

$$\boldsymbol{N}_2 = \begin{pmatrix} 0 \\ 0 \\ -1-q \end{pmatrix}.$$

The locus of the optimum switching points for various values of A is called the optimum switching curve. Furthermore varying B, the corresponding optimum switching curves make the surface in the $z_1z_2z_3$ space, which is called the optimum switching surface. The equation of the surface is

$$h(z_1,\ z_2,\ z_3) = 0\,. \tag{17}$$

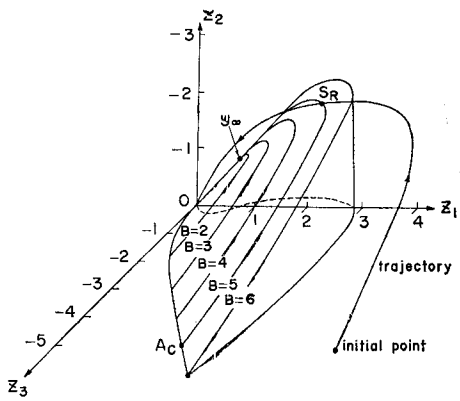

Fig. 3. The optimum switching surface and the phase trajectory in the $z_1z_2z_3$ space for a system with $\zeta=1.2$ and $q=0.2$

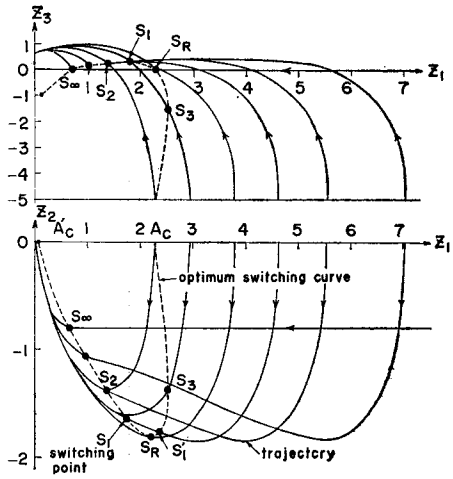

Fig. 4. Projection of the optimum switching curve and the phase trajectories on the z_1z_2 and z_1z_3 planes for a system with $\zeta=1.2$ and $q=0.2$

Fig. 3 shows the optimum switching surface for $\zeta=1.2$ and $q=0.2$. Fig. 4 shows the projections of the optimum switching curve and the optimum phase trajectories for $\zeta=1.2$, $q=0.2$ and $B=5$ on the z_1z_2 and z_1z_3 planes.

The optimum switching curve is $S_\infty S_R A_C$ shown by the broken line which is for the case of $B>(q-1)/\lambda_1$ and S_∞ is the switching point for $A=\infty$. The switching points move from S_∞ to S_R according as the initial points approach the terminal position. At the switching on the curve $S_\infty S_R$, z_3's are positive. When $A=A_R$, the switching is performed at S_R on the switching curve where $z_3=0$. The switching points move from S_R to A_C according as the initial points approach the terminal position over A_R. z_3's become negative at the switching points in this case.

Therefore, when the phase trajectroies intersect the optimum switching curve in the z_1z_2 plane, the controls should be switched from $u=1$ to $u=-1$ on the curve $S_\infty S_R$ and $S_R A_C$ according to $z_3>0$ and $z_3<0$ at the switching point, respectively. When $A=A_C$, the controller must be switched simultaneously with the start of the motion. When $\overline{OA}<\overline{OA_C}$, in spite of simultaneous switching, the load cannot be transported to $z_1=0$, $z_2=0$ and it overshoots the terminal position. The region $\overline{OA_C}$ is called the uncontrollable region.

In the case of $B\leq(q-1)/\lambda_1$, the optimum switching curves on the z_1z_2 plane have no bottoms and the forward trajectory intersects the specific switching curve only once. The switching points move from S_∞ to A_C' as the initial points approach the terminal position. Therefore, when $B\leq(q-1)/\lambda_1$, the optimum switching points can be determined uniquely on the z_1z_2 plane.

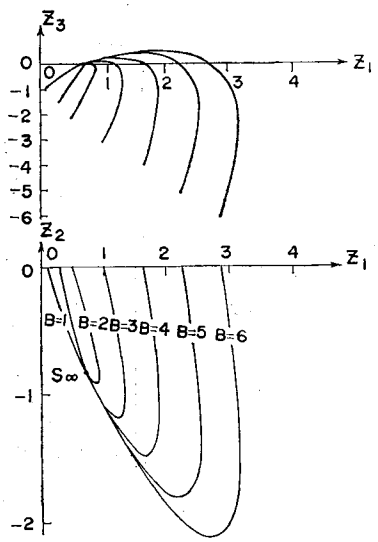

Fig. 5. Relation between optimum switching curves and B

The optimum switching curves for the various initial acceleration B are shown in Fig. 5. The uncontrollable region decreases as B does. This means that the difference between the static and dynamic friction forces must be decreased and the rigidity of the system must be increased to obtain the high accuracy control.

In the above discussions, we assume $|u| \leq 1$ which means that the forward and the reverse controls have the same magnitudes and the opposite signs. Next, we discuss the case where both controls have different magnitudes.

In Fig. 6, the optimum trajectories and the optimum switching curve with $|\bar{u}| = 5.8\ u$ are shown where other parameters are the same as in Fig. 4. The optimum switching curve approaches the z_1 axis and the switching takes place at a nearer point than the case of $|\bar{u}| = u$. The uncontrollable region $\overline{OA}_C$ is remarkably

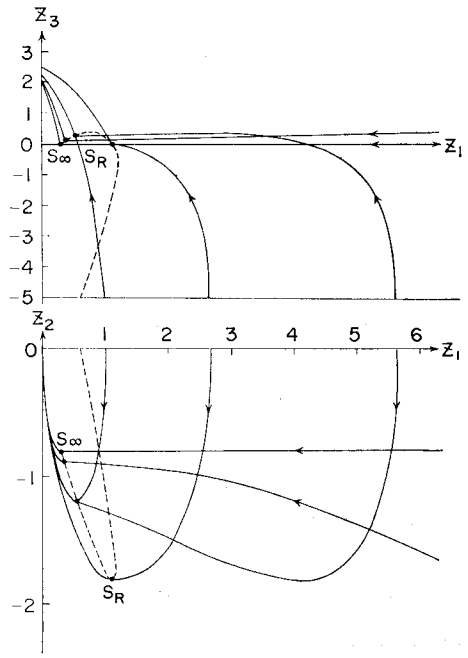

Fig. 6. Projection of the optimum switching curve and the phase trajectories on the z_1z_2 and z_1z_3 planes for a system with $\zeta=1.2$, $q=0.2$ and $B=5$, when $u=1$ and $\bar{u}=5.8$

reduced and high accuracy can be obtained. However, extremely strong reverse control stops the load so rapidly that the terminal acceleration exceeds the limit of Eq. (5) and the load turns back after the stop.

Inversely, the small reverse control increases the uncontrollable region. Fig. 7 shows the optimum trajectories and the optimum switching curve for $\bar{u}=0$. This

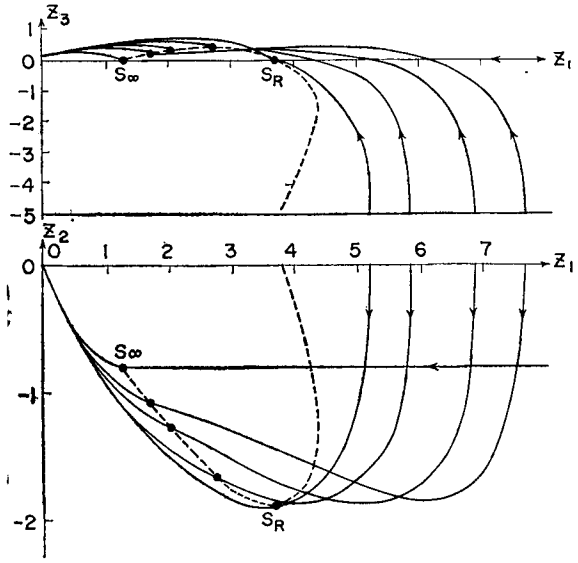

Fig. 7. Projection of the optimum switching curve and the phase trajectories on the z_1z_2 and z_1z_3 planes for a system with $\zeta=1.2$, $q=0.2$ and $B=5$, when $u=1$ and $\bar{u}=0$

control can be achieved only by switching off the controller prior to the terminal position and is often used because of the simplicity of the device. But it cannot avoid the wide uncontrollable region and so the less control accuracy.

The limit point A_C of the controllable region can be determined by the trajectories which are obtained by substituting $u=-u_M$ into Eq. (1) at $\tau=0$, where u_M is the maximum absolute value of the reverse control.

When $\zeta=1$, the trajectories are similar to the case of $\zeta>1$ and the controls are determined by similar ways as before.

4. Time Optimum Control of the System with $\zeta<1$

4.1 Occurrence of Stick-slip

When $\zeta<1$, the characteristic equation of Eq. (1) has complex roots and the motion of load is oscillatory. This means the possibility of stick-slip.[7] Eq. (2) is transformed as follows,

$$\begin{aligned}\frac{dy_1}{d\tau} &= -\zeta y_1-\omega y_2+(u-q)\\ \frac{dy_2}{d\tau} &= \omega y_1-\zeta y_2\\ \frac{dy_3}{d\tau} &= u-q\,,\end{aligned} \tag{18}$$

where

$$\begin{aligned} y_1 &= -\zeta z_2 - z_3 \\ y_2 &= -\omega z_2 \\ y_3 &= -z_1 - 2\zeta z_2 - z_3\,, \quad \omega = (1-\zeta^2)^{1/2} \end{aligned} \tag{19}$$

From Eqs. (3) and (19), the initial conditions of Eq. (18) become as

$$y_{10} = B\,, \quad y_{20} = 0 \quad \text{and} \quad y_{30} = B - A\,. \tag{20}$$

The forward trajectories on the $y_1 y_2$ plane are obtained as follows, substituting $u=1$ in Eq. (18).

$$\frac{dy_1}{dy_2} = \frac{-\zeta y_1 - \omega y_2 + Q}{\omega y_1 - \zeta y_2}, \tag{21}$$

where

$$Q = 1 - q\,.$$

Using $y_1 - \zeta Q = r\cos\theta$, $y_2 - \omega Q = r\sin\theta$ and the initial conditions of Eq. (20), we obtain

$$r = (B^2 - 2B\zeta Q + Q^2)^{1/2} \exp\left\{-\frac{\zeta}{\omega}(\theta - \theta_0)\right\}, \tag{22}$$

where

$$\theta_0 = \tan^{-1}\left(\frac{\omega Q}{\zeta Q - B}\right), \qquad -\pi < \theta_0 < 0$$

From Eq. (22), the forward trajectories are the logarithmic spirals which have the center at $0_1(\zeta Q, \omega Q)$, start from the point on the y_1 axis and rotate counter-clockwise with τ. Fig. 8 shows the case of $\zeta=0.2$, $q=0.2$, $B=2$ and $B=5$.

The condition of the occurrence of stick-slip is discussed now. y_2 is proportional to the velocity because $y_2 = -\omega z_2$. The load stops when the trajectory intersects the y_1 axis. As soon as the motion stops, the static friction acts on the load. The load stops until the driving force overcomes the static friction. The load repeats the stick and the slip. The existence of stick-slip depends on whether the trajectory intersects the y_1 axis or not.

In Fig. 8, the forward trajectory for $B=2$ starts from $y_1=2$, and goes toward O_1. In this case, no stick-slip occurs and the velocity approaches the constant value after the damped oscillation. The trajectory for $B=5$ starts from $y_1=5$ and goes as $M\,S_1\,S_2\,S_3\,S_L$. y_2 becomes zero at S_L and the motion stops. The condition of the occurrence of stick-slip is given by $y_{2\min.} \leq 0$. Substituting Eq. (22) in $y_2 = \omega Q + r\sin\theta$, the minimum value of y_2 is obtained. The condition for $y_{2\min.} \leq 0$ becomes

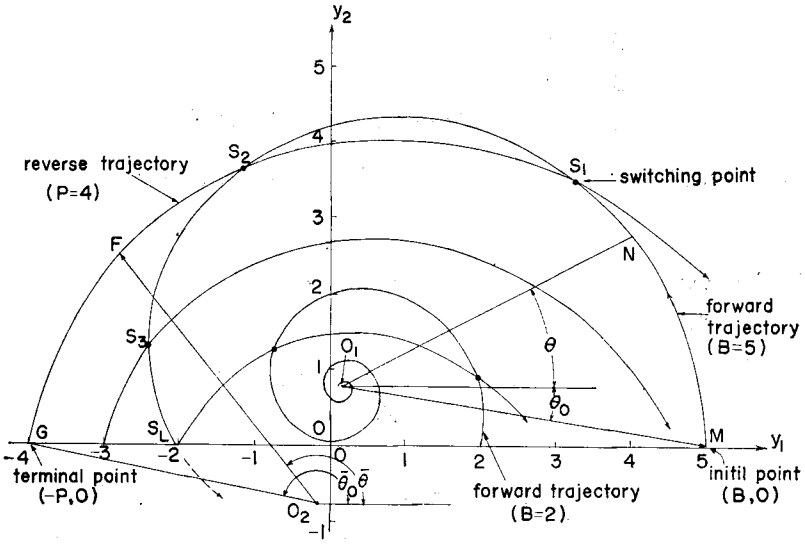

Fig. 8. Projection of the forward and the reverse trajectories on the y_1y_2 plane for a system with $\zeta=0.2$ and $q=0.2$

$$(B^2-2B\zeta Q+Q^2)^{1/2}\left\{\exp\left(-\frac{\zeta}{\omega}\tan^{-1}\frac{B\omega}{B\zeta-Q}\right)\right\}\geq Q\,, \tag{23}$$

where

$$\pi<\tan^{-1}\frac{B\omega}{B\zeta-Q}<2\pi\,.$$

4.2 Control by One Time Switching

When $\zeta<1$, multiple switchings of the controller are necessary to realize the optimum control in general.[8)9)] However, we consider one time switching of the controller for the simple construction of the control system.

The switching is carried out at the intersection of the forward and the reverse trajectory. The forward trajectories are given by Eq. (22). The reverse trajectories in the y_1y_2 plane are obtained in the same way as the forward trajectories under the terminal condition,

$$y_{1T}=-P\,,\quad y_{2T}=0\quad\text{and}\quad y_{3T}=-P\,.$$

They are the logarithmic spirals which have the center at $O_2(-\zeta Q,\,-\omega Q)$, start from the point on the y_1 axis and rotate clockwise according to the increase of the reverse time $\bar{\tau}$ as shown in Fig. 8. The switching points are the intersections of the forward and reverse trajectories in the $y_1y_2y_3$ space. For example, the point S_1 is the switching point for $A=8$ and $B=5$, and S_2 for $A=10$ and $B=5$. If the

controller is switched at this point, the load can be transported to $z_1=0$, $z_2=0$ and the terminal acceleration $P=4$.

(1) The case when stick-slip occurs

When stick-slip occurs, the load repeats the same motion intermittently. The problem exists in the final step which involves the terminal position. Fig. 9 is the projection of the phase trajectories and the optimum switching curve on the z_1z_2 and z_1z_3 planes for $\zeta=0.2$, $q=0.2$ and $B=5$. In this case, the control is

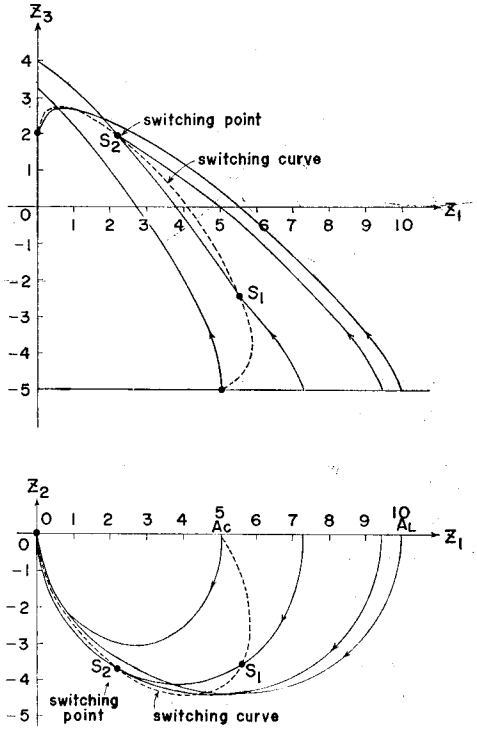

Fig. 9. Projection of the optimum switching curve and the phase trajectories on the z_1z_2 and z_1z_3 planes for a stick-slip motion ($\zeta=0.2$, $q=0.2$ and $B=5$)

determined in a way similar to the case of $\zeta\geq 1$. When $A=A_L$, the trajectories enter $z_1=0$ and $z_2=0$ with $u=1$. This means that OA_L is the displacement of the one step of stick-slip. A_C is the limit of controllable region which exists intermittently as

$$m\cdot\overline{OA}_C\leq A\leq m\cdot\overline{OA}_L \qquad (m=1, 2,\cdots)\,.$$

(2) The case when no stick-slip occurs

Fig. 10 is the projection of the trajectories and the optimum switching curve

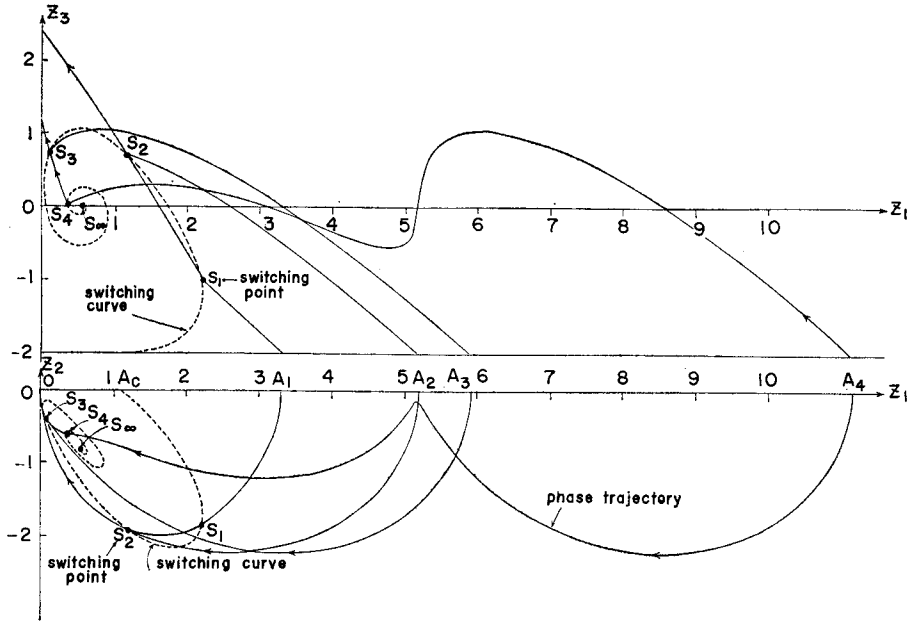

Fig. 10. Projection of the optimum switching curve and the phase trajectories on the z_1z_2 and z_1z_3 planes for a system with no stick-slip motion ($\zeta=0.2$, $q=0.2$ and $B=2$)

on the z_1z_2 and z_1z_3 planes for $\zeta=0.2$, $q=0.2$ and $B=2$. On the z_1z_2 plane, the switching curve is the spiral which starts from A_C on the z_1 axis and approaches the center S_∞. The forward trajectories start from the points on the z_1 axis and approach the terminal position with damped oscillations and intersect the switching curve. The forward trajectories intersect with the switching curve at many points apparent in the z_1z_2 plane, but the real intersection is only one in the $z_1z_2z_3$ space. The switching point goes to the center of the spiral as A_C, S_1, S_2, $\cdots$ according as the initial point goes away from A_C, as A_1, A_2, $\cdots$. S_∞ is the switching point for the trajectory which starts from the infinite distance.

4.3 Discussion about Optimality

The maximum principle gives the necessary and sufficient condition for the time optimum control of the system which is linear and has the additive control function.[6] Consequently, if the control of the above one time switching maximizes Hamiltonian H, optimality is guaranteed.

We use Hamiltonian $\bar{H}$ with the reverse time $\bar{\tau}$ instead of H in this case. $\bar{H}$ is

$$\bar{H} = -1+\{\zeta\bar{y}_1+\omega\bar{y}_2-(u-q)\}\bar{\psi}_1+(-\omega\bar{y}_1+\zeta\bar{y}_2)\bar{\psi}_2-(u-q)\bar{\psi}_3\,, \qquad (24)$$

where

$$\begin{aligned} d\bar{\psi}_1/d\bar{\tau} &= -\partial\bar{H}/\partial\bar{y}_1 = -\zeta\bar{\psi}_1+\omega\bar{\psi}_2\,, \\ d\bar{\psi}_2/d\bar{\tau} &= -\partial\bar{H}/\partial\bar{y}_2 = -\omega\bar{\psi}_1+\zeta\bar{\psi}_2\,, \\ d\bar{\psi}_3/d\bar{\tau} &= -\partial\bar{H}/\partial\bar{y}_3 = 0\,. \end{aligned} \tag{25}$$

Solving Eq. (25),

$$\begin{aligned} \bar{\psi}_1(\bar{\tau}) &= (\bar{\psi}_{10}\cos\omega\bar{\tau}+\bar{\psi}_{20}\sin\omega\bar{\tau})\exp(-\zeta\bar{\tau})\,, \\ \bar{\psi}_2(\bar{\tau}) &= (-\bar{\psi}_{10}\sin\omega\bar{\tau}+\bar{\psi}_{20}\cos\omega\bar{\tau})\exp(-\zeta\bar{\tau})\,, \\ \bar{\psi}_3(\bar{\tau}) &= \bar{\psi}_{30}\,. \end{aligned} \tag{26}$$

From the condition of maximizing Eq. (24), the optimum control $\bar{u}$ is obtained as follows.

$$\bar{u} = -\mathrm{sgn}\,(\bar{\psi}_1+\bar{\psi}_3) = -\mathrm{sgn}\,\{(\bar{\psi}_{10}\cos\omega\bar{\tau}+\bar{\psi}_{20}\sin\omega\bar{\tau})\exp(-\zeta\bar{\tau})+\bar{\psi}_{30}\}\,. \tag{27}$$

It is obvious that $u=1$ at the initial point (i.e. the terminal point in the reverse time) and it means

$$-1+B\zeta\bar{\psi}_{1T}-B\omega\bar{\psi}_{2T}-Q(\bar{\psi}_{1T}+\bar{\psi}_{3T}) = 0\,. \tag{28}$$

From the transversality condition at the terminal point,

$$\bar{\psi}_{10}+\bar{\psi}_{30} = 0\,. \tag{29}$$

The maximum value of $\bar{H}$ should be zero because T is not determined. This means

$$-1-P\zeta\bar{\psi}_{10}+P\omega\bar{\psi}_{20} = 0 \tag{30}$$

at the terminal point.

Obtaining $\bar{\psi}_{10}$, $\bar{\psi}_{20}$ and $\bar{\psi}_{30}$ from Eqs. (28), (29) and (30) and substituting them into Eq. (27),

$$u = -\mathrm{sgn}\,\{g(\bar{\tau})\}\,, \tag{31}$$

where

$$g(\bar{\tau}) = e^{-\zeta\bar{\tau}}\cos(\omega\bar{\tau}-\alpha)-\cos\alpha\,, \tag{32}$$

$$\alpha = \tan^{-1}\frac{\zeta P+e^{-\zeta T}\{B\omega\sin\omega T+(B\zeta-Q)\cos\omega T\}+Q}{\omega P+e^{-\zeta T}\{B\omega\cos\omega T-(B\zeta-Q)\sin\omega T\}}\,. \tag{33}$$

The switching times are represented by τ_s and $\bar{\tau}_s$ in the forward and the reverse time, respectively. Then

$$T = \tau_s+\bar{\tau}_s\,. \tag{34}$$

Substituting Eqs. (33) and (34) into Eq. (32) and eliminating τ_s by using the relation between τ_s and $\bar{\tau}_s$ obtained from Eq. (2),

$$g(\bar{\tau}) = \frac{2(e^{-\zeta\bar{\tau}} \sin \omega\bar{\tau} - e^{-\zeta\bar{\tau}_s} \sin \omega\bar{\tau}_s) - 2e^{-\zeta(\bar{\tau}+\bar{\tau}_s)} \sin \omega(\bar{\tau}-\bar{\tau}_s)}{\omega P + e^{-\zeta T}\{B\omega \cos\omega T - (B\zeta - Q) \sin \omega T\}} \cos \alpha \,. \tag{35}$$

Now the sign of $g(\bar{\tau})$ is examined. The denominator of Eq. (35) can be rewritten as $\omega\{P - z_3(T)\}$, where $z_3(T)$ is obtained from Eq. (2) and

$$z_3(T) = \{(B\zeta - Q) \sin \omega T - B\omega \cos \omega T\} \exp(-\zeta T)/\omega \,.$$

From numerical calculation, $P - z_3(T) > 0$ and the denominator of $g(\bar{\tau})$ is positive.

Next, the sign of $\cos\alpha$ in Eq. (35) is examined. The denominator of Eq. (33) is the same as Eq. (35) and is positive. The numerator of Eq. (33) is rewritten as $\zeta\{P - z_3(T)\} - z_2(T)$, where $z_2(T)$ is obtained from Eq. (2). Since $P - z_3(T) > 0$ and $-z_2(T) > 0$, $\tan\alpha > 0$ and $0 < \alpha < \pi/2$ from Eq. (33). This means $\cos\alpha > 0$.

Consequently, Eq. (31) is reduced to the following:

$$u = -\mathrm{sgn}\{f(\bar{\tau})\} \,, \tag{36}$$

where

$$f(\bar{\tau}) = e^{-\zeta\bar{\tau}} \sin \omega\bar{\tau} - e^{-\zeta\bar{\tau}_s} \sin \omega\bar{\tau}_s - e^{-\zeta(\bar{\tau}+\bar{\tau}_s)} \sin \omega(\bar{\tau}-\bar{\tau}_s) \,. \tag{37}$$

Fig. 11 shows $f(\bar{\tau})$ in the reverse time. $f(\bar{\tau}) = 0$ at $\bar{\tau} = \bar{\tau}_s$ because the switching occurs at this moment. Therefore, if the change of the sign of $f(\bar{\tau})$ does not occur during $\bar{\tau}_s < \bar{\tau} < T$, the one time switching control is time optimal.

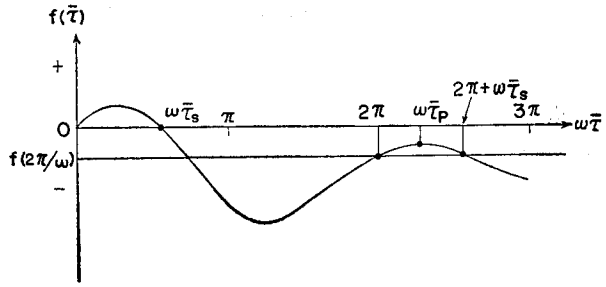

Fig. 11. Sketch of the behavior of $f(\bar{\tau})$ vs. $\bar{\tau}$

First, when stick-slip occurs, the relation between the angle θ of the forward trajectory in the y_1y_2 plane of Fig. 8 and τ is

$$\tau = (\theta - \theta_0)/\omega \,. \tag{38}$$

For example, the time τ_n at N on the trajectory starting from $y_1 = 5$ is given by $\angle NO_1M/\omega$. Also on the reverse trajectory,

$$\bar{\tau} = (\bar{\theta}_0 - \bar{\theta})/\omega \,. \tag{39}$$

From this, the total control period T is given by $T = (\angle S_2O_1M + \angle S_2O_2G)/\omega$ where

S_2 is the switching point. In this case, $T<2\pi/\omega$ obviously from the figure. At $\bar{\tau}=2\pi/\omega, f(2\pi/\omega)=e^{-\zeta\bar{\tau}_s}\sin\omega\bar{\tau}_s(e^{-2\pi\zeta/\omega}-1)$. Therefore, $f(2\pi/\omega)<0$ for $0<\omega\bar{\tau}_s<\pi$. τ_p which represents the time at the second peak of $f(\bar{\tau})$ is larger than $2\pi/\omega$. $f(\bar{\tau})=0$ occurs only at $\bar{\tau}=\bar{\tau}_s$ during $0<\bar{\tau}\leq T$. Optimality of the one time switching control is ensured in this case.

Next, when no stick-slip occurs, the forward trajectory comes near 0_1 in Fig. 8 asymptotically and T takes all values according to the initial conditions.

When $0<T<2\pi/\omega$, optimality is ensured as well as in the case with the stick-slip. When $T>2\pi/\omega$, optimality is guaranteed for all initial conditions only if $f(\bar{\tau})<0$ at $\bar{\tau}<\bar{\tau}_s$. This condition is given by $f(\bar{\tau}_p)<0$ and it becomes from Eq. (37) as follows:

$$f(\bar{\tau}_p)=\omega(1-2e^{-\zeta\bar{\tau}_s}\cos\omega\bar{\tau}_s+e^{-2\zeta\bar{\tau}_s})^{1/2}e^{-\zeta\bar{\tau}_p}-e^{\zeta\bar{\tau}_s}\sin\omega\bar{\tau}_s<0\,, \tag{40}$$

where

$$\omega\bar{\tau}_p=\tan^{-1}\frac{\omega-e^{-\zeta\bar{\tau}_s}(\zeta\sin\omega\bar{\tau}_s+\omega\cos\omega\bar{\tau}_s)}{\zeta-e^{-\zeta\bar{\tau}_s}(\zeta\cos\omega\bar{\tau}_s-\omega\sin\omega\bar{\tau}_s($$

$$2\pi<\omega\bar{\tau}_p<3\pi\,.$$

$f(\bar{\tau}_p)$ is the function of ζ and $\bar{\tau}_s$. $\bar{\tau}_s$ depends on A and B, so $f(\bar{\tau}_p)$ is the function of A and B. Fig. 12 shows the critical condition between B and ζ of $f(\bar{\tau}_p)\leq 0$ and the occurrence of stick-slip given by Eq. (23). Optimality is not always guaranteed in the shaded region which exists for $\zeta<0.05$. However, this condition scarcely occurs in practice.

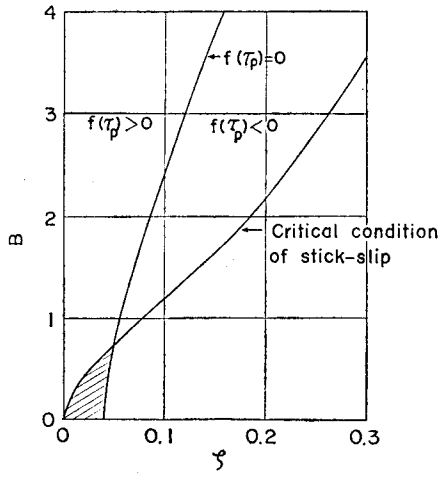

Fig. 12. Region where the optimality is guaranteed

5. Sensitivity Analysis

The optimum switching curves are obtained for an ideal mathematical model. But in practical use, the sensitivity which means the effect of the changes of parameters to the control accuracy should be considered.

The terminal error which occurs when the controller is switched at the different point from the optimum switching point is investigated. The terminal error means the position deviation of the load position from the terminal position where the velocity equals to zero.

The forward and the reverse trajectories shown by Eqs. (15) and (16) represented as follows:

$$\boldsymbol{Z}(\tau) = \boldsymbol{F}_1(\tau)+\boldsymbol{G}_1(\tau)B+\begin{pmatrix} A \\ 0 \\ 0 \end{pmatrix} \tag{41}$$

$$\boldsymbol{Z}(\bar{\tau}) = \boldsymbol{F}_2(\bar{\tau})+\boldsymbol{G}_2(\bar{\tau})P \tag{42}$$

If the terminal positions are given by $z_{1T}=\alpha$, $z_{2T}=0$ and $z_{3T}=P$ instead of $z_{1T}=0$, $z_{2T}=0$ and $z_{3T}=P$, the reverse trajectory becomes

$$\boldsymbol{Z}(\bar{\tau}) = \boldsymbol{F}_2(\bar{\tau})+\boldsymbol{G}_2(\bar{\tau})P+\begin{pmatrix} \alpha \\ 0 \\ 0 \end{pmatrix}. \tag{43}$$

Substituting $z_1-\alpha=z_1'$, Eq. (43) reduces to Eq. (42). Therefore, the optimum switching surface is the same form given by Eq. (17), that is,

$$h(z_1-\alpha,\ z_1,\ z_2) = 0\,. \tag{44}$$

That is obtained by moving the switching surface of $h(z_1,\ z_2,\ z_3)=0$ by α along the z_1 axis. In other words, the terminal error α is equal to the distance along the z_1 axis from the actual switching point to the optimum switching point.

The deviation of the optimum switching point caused by the change of initial condition is obtained as follows. The suffix op indicates the values at the normal optimum switching point. The optimum switching point is expressed as $\boldsymbol{Z}_{op}$ when the initial condition is expressed as $\boldsymbol{Z}_0$.

When the initial conditions change slightly from $\boldsymbol{Z}_0$ to $\boldsymbol{Z}_0+\Delta\boldsymbol{Z}_0$, each state variables slightly changes from the normal values. The following equation is obtained from Eq. (15).

$$\boldsymbol{Z}_{op}+\Delta\boldsymbol{Z}_{op} = \boldsymbol{\phi}(\tau_{op}+\Delta\tau_{op})(\boldsymbol{Z}_0+\Delta\boldsymbol{Z}_0)+\int_0^{\tau_{op}+\Delta\tau_{op}}\boldsymbol{\phi}(\tau_{op}+\Delta\tau_{op}-s)\boldsymbol{N}_1\,ds$$

Therefore the equation about small variables is obtained as follows:

$$\Delta \boldsymbol{Z}_{op} = \{\boldsymbol{M}\boldsymbol{\phi}(\tau_{op})\boldsymbol{Z}_0+\boldsymbol{\phi}(\tau_{op})\boldsymbol{N}_1\}\Delta\tau_{op}+\boldsymbol{\phi}(\tau_{op})\boldsymbol{Z}_0 . \tag{45}$$

Because, neglecting the second order small variables and using Taylor expansion,

$$\boldsymbol{\phi}(\tau_{op}+\Delta\tau_{op})(\boldsymbol{Z}_0+\Delta\boldsymbol{Z}_0) = \boldsymbol{\phi}(\tau_{op})\boldsymbol{Z}_0+\boldsymbol{M}\boldsymbol{\phi}(\tau_{op})\boldsymbol{Z}_0\Delta\tau_{op}+\boldsymbol{\phi}(\tau_{op})\Delta\boldsymbol{Z}_0 ,$$

$$\begin{aligned}\int_0^{\tau_{op}+\Delta\tau_{op}} \boldsymbol{\phi}(\tau_{op}+\Delta\tau_{op}-s)\boldsymbol{N}_1 ds &= \int_0^{\tau_{op}} (\tau_{op}-s)\boldsymbol{N}_1+\frac{\partial}{\partial t}\left[\int_0^t \boldsymbol{\phi}(t-s)\boldsymbol{N}_1 ds\right]_{t=\tau_{op}}\Delta\tau_{op} \\ &= \int_0^{\tau_{op}} \boldsymbol{\phi}(\tau_{op}-s)\boldsymbol{N}_1\, ds+\int_0^{\tau_{op}} \boldsymbol{M}\boldsymbol{\phi}(\tau_{op}-s)\boldsymbol{N}_1\, ds\,\Delta\tau_{op} \\ &\quad +\boldsymbol{N}_1\Delta\tau_{op} \\ &= \int_0^{\tau_{op}} \boldsymbol{\phi}(\tau_{op}-s)\boldsymbol{N}_1\, ds+\boldsymbol{\phi}(\tau_{op})\boldsymbol{N}_1\Delta\tau_{op} ,\end{aligned}$$

and

$$\boldsymbol{Z}_{op} = \boldsymbol{\phi}(\tau_{op})\boldsymbol{Z}_0+\int_0^{\tau_{op}} \boldsymbol{\phi}(\tau_{op}-s)\boldsymbol{N}_1 ds .$$

The similar equation in the reverse time is obtained in the same way.

$$\Delta\bar{\boldsymbol{Z}}_{op} = \{-\boldsymbol{M}\boldsymbol{\phi}(-\bar{\tau}_{op})\boldsymbol{Z}_T+\boldsymbol{\phi}(-\bar{\tau}_{op})\boldsymbol{N}_2\}\Delta\bar{\tau}_{op}+\boldsymbol{\phi}(-\bar{\tau}_{op})\Delta\boldsymbol{Z}_T . \tag{46}$$

$\Delta\tau_{op}$ is obtained by $\Delta\boldsymbol{Z}_{op}=\Delta\bar{\boldsymbol{Z}}_{op}$. Substituting $\Delta\tau_{op}$ in Eq. (45), the variation of the optimum switching point $\Delta\boldsymbol{Z}_{op}$ is obtained.

Now, we consider the variation of B due to the change of friction force. Fig. 13 shows the relation between the terminal error and the optimum switching curve for the change of B from B_0 to $B_0+\Delta B$. The solid lines show the optimum

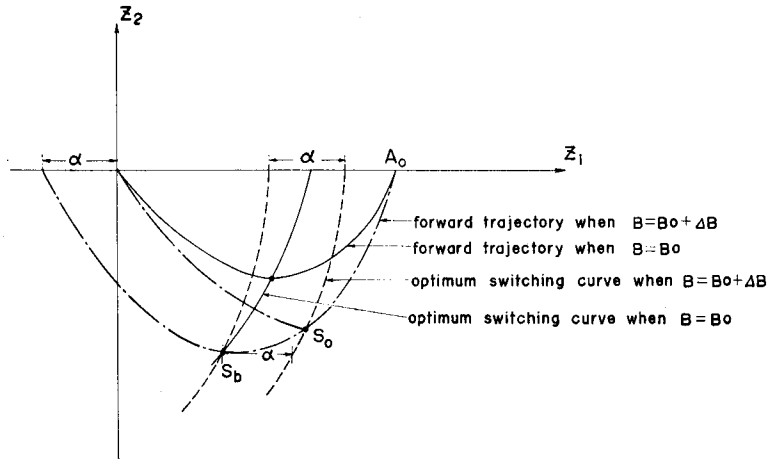

Fig. 13. Terminal error due to a change of B

switching curve and the trajectory in the case of $B=B_0$. The optimum switching point is S_0 for $B=B_0+\Delta B$, but the controller is actually switched at the point S_b because B is estimated as B_0. The terminal error caused by this switching delay is given as the horizontal distance α from the point S_b to the optimum switching curve.

Fig. 14 shows the relation between $(\partial\alpha/\partial B)_{B_0}$ which represents the sensitivity of the terminal error to B. It depends on A. The normal optimum switching curves and the optimum trajectories are also shown. $B_0=5$ and $B_0=1$ are considered as the normal value and other parameters are same as Fig. 4. When $B_0=1$, $(\partial\alpha/\partial B)_{B_0}$ is small for all initial points. The control accuracy is not much affected by the variation of B and the high accuracy control is possible.

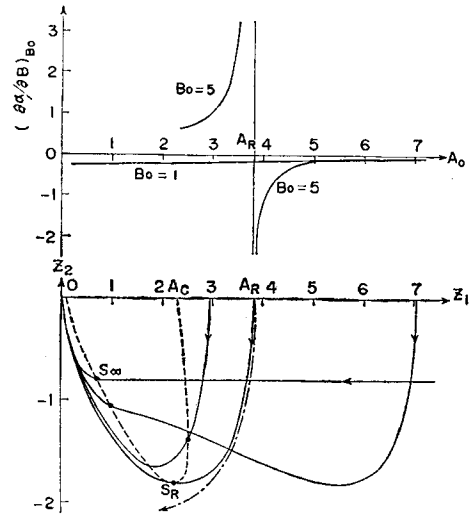

Fig. 14. Sensitivities to initial points for $\zeta=1.2$, $q=0.2$ and $B=1,5$

Conversely, $(\partial\alpha/\partial B)_{B_0}$ is relatively large for $B_0=5$ and it becomes infinite at $A=A_R$. This means that the trajectory from A_R cannot intersect the optimum switching curve when B changes slightly. This is evident from the figure. The region near $A=A_R$ is a kind of uncontrollable region. The uncontrollable region should be avoided in practical control systems. Therefore, the switching curve on the z_1z_2 plane is not favorable in the meaning of the sensitivity as well as the difficulty of its realization. The following two quasi-optimization methods are presented to avoid the contradiction of the optimum control.

6. Quasi-optimum Controls

6.1 Quasi-optimum switching line

This method intends to obtain the quasi-optimum control by approximating the optimum switching curve projected on the z_1z_2 plane by a straight line. This means the control by a conventional position-plus-velocity feedback.

The optimum switching curve for $\zeta \geq 1$ and $B>(q-1)/\lambda_1$ is approximated by two lines. Fig. 15 shows the trajectories in the case of $\zeta=1.2$, $q=0.2$ and $B=5$. The controller should be switched by the line ① which passes through 0 and S_∞, if z_3 is positive at the intersection of the forward trajectory and the optimum switching line. The other switching line ② which is perpendicular to the z_1 axis and passes through A_C is used if z_3 is negative at the intersection. The control should be zero when the velocity becomes zero. When the line ① is used, the terminal error is maximum for $A=A_R$. When the line ② is used, the switching point becomes

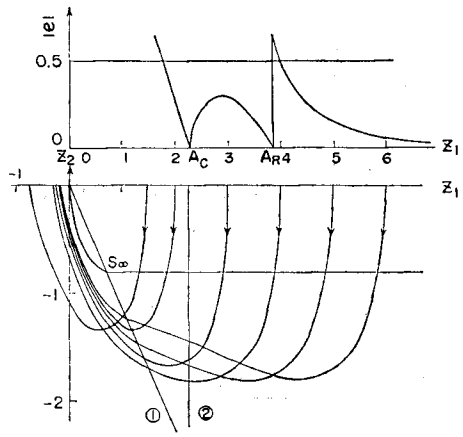

Fig. 15. Trajectories of quasi-optimum controls by using quasi-optimum switching lines for $\zeta=1.2$, $q=0.2$ and $B=5$

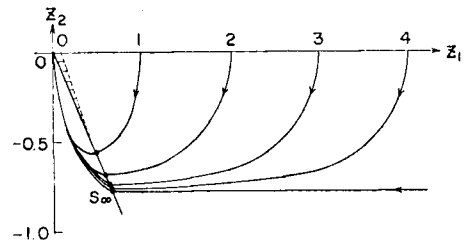

Fig. 16. Trajectories of quasi-optimum controls by using quasi-optimum switching line for $\zeta=1.2$, $q=0.2$ and $B=1$

optimum for $A=A_C$ and $A=A_R$. The terminal error is very small for $\overline{OA}_C<A<\overline{OA}_R$ and the control is almost optimum.

The optimum switching curve has not the peak when $B\leq(q-1)/\lambda_1$ and it is approximated by a single switching line. Fig. 16 shows the case of $\zeta=1.2$, $q=$

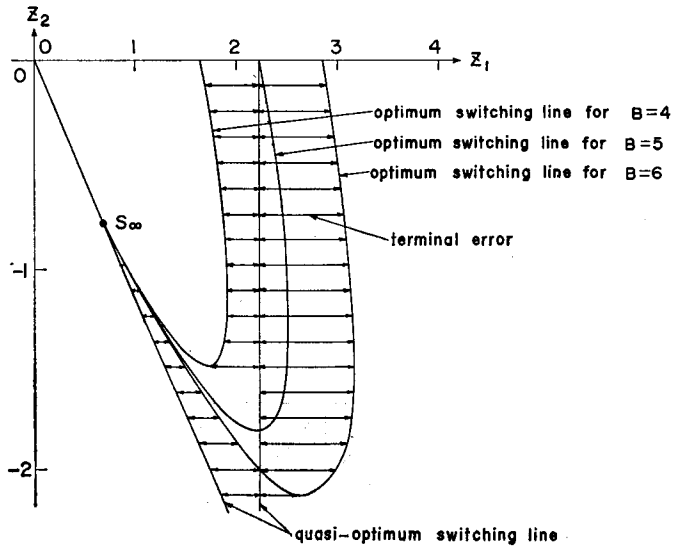

Fig. 17. Sensitivities of quasi-optimum switching for $\zeta=1.2$, $q=0.2$ and $B=5\pm1$

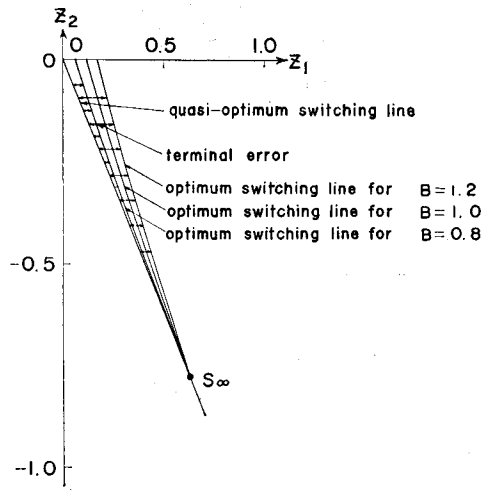

Fig. 18. Sensitivities of quasi-optimum switching for $\zeta=1.2$, $q=0.2$ and $B=1\pm0.2$

0.2 and $B=1$. In this case, the switching points are determined uniquely by the intersections of the forward trajectories and the switching line. The terminal error is very small for all initial points.

Next, we study the sensitivity to the parameters variation in the system. As an example, we consider the case when the initial acceleration B changes by $\pm 20\%$ from the normal value. Fig. 17 and Fig. 18 shows the terminal error for $B=5\pm 1$ and $B=1\pm 0.2$, respectively (both for $\zeta=1.2$ and $q=0.2$). The relatively large error occurs for some initial points in the case of $B>(q-1)/\lambda_1$, while the terminal error is small for all initial points in the case of $B\leq(q-1)/\lambda_1$. The approximation by the switching line is very effective especially in $B\leq(q-1)/\lambda_1$.

6.2 Quasi-optimum switchin plane

As previously described, the optimum switching curves construct the optimum switching surface. Now, the surface is approximated by a simple plane. This means the quasi-optimum control by the acceleration feedback in addition to the conventional position-plus-velocity feedback.

The surface in Fig. 3 is approximated by the plane which is determined by S_∞, S_R and A_C in Fig. 19. The co-ordinates of S_∞, S_R and A_C are obtained by Fig. 3 and they are given by $(s_1, s_2, 0)$, $(r_1, r_2, 0)$ and $(a_1, 0, a_3)$, respectively. The equation of the plane is as follows:

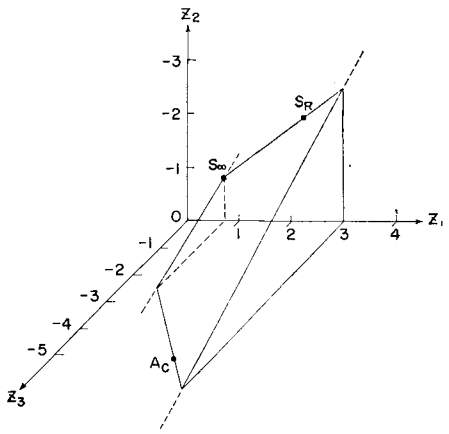

Fig. 19. The quasi-optimum switching plane for $\zeta=1.2$ and $q=0.2$

$$\begin{vmatrix} z_1, & z_2, & z_3, & 1 \\ s_1, & s_2, & 0, & 1 \\ a_1, & 0, & a_3, & 1 \end{vmatrix} = 0 . \tag{47}$$

This plane approximates the surface well in the case of $B>(q-1)/\lambda_1$.

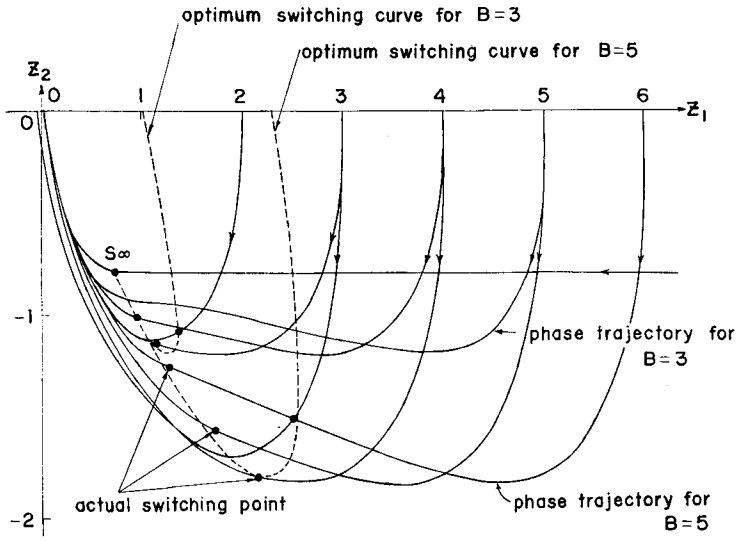

Fig. 20. Switching points and the phase trajectories of quasi-optimum controls by using the quasi-optimum switching plane for $\zeta=1.2$, $q=0.2$ and $B=3,5$

Fig. 20 shows the phase trajectories and the switching points by such quasi-optimum control. B is chosen as 5 and 3, and the other paraters are same as Fig. 4. They correspond to the case of $B>(q-1)/\lambda_1$. In the figure, the optimum switching curves are shown for $B=5$ and $B=3$. Little differences exist between the actual and optimum switching points. The terminal error due to the variation of the parameters is so small that this method is very effective.

In the case of $B\leq(q-1)/\lambda_1$, the quasi-optimum control by the switching plane is performed more easily than the previous case. Although the acceleration feedback is somewhat difficult, we can obtain the same effect by the pressure feedback instead of the acceleration feedback in a hydraulic control system.

The above description concerns the case of $\zeta\geq 1$. For $\zeta<1$, the optimum control is performed by the very complicated switching surface. But we might obtain the quasi-optimum control by the proper choice of the switching plane.

7. Experiment

7.1 Experimental equipment

The structure of the experimental equipment is shown in Fig. 21. The position of load is detected by the differential transformer. The analog computer is used for the controller and drives the servo valve by the output directly. The cylinder bore is of 35.6 mm and the piston has double rods. The high pressure

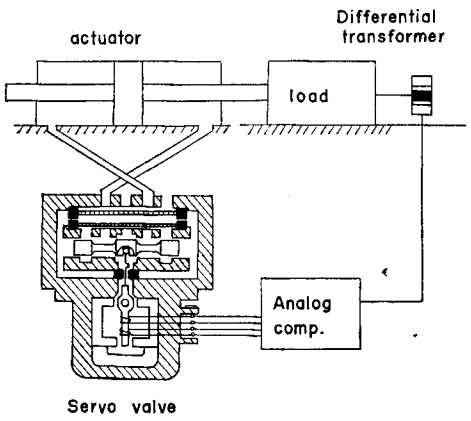

Fig. 21. Valve-controlled electro-hydraulic servomechanism

rubber hoses are used for the connection of the servo valve and the actuator. This increases the compliance of the system and makes the control difficult.

The dimensions of the control system are following.

A_p	= 10	cm^2	B	= 0.99	
M_p	= 0.143	kg sec^2/cm	F_s	= 120	kg
k_1	= 2.31	cm^3/mA sec	F_v	= 90	kg
k_2	= 0.465	cm^5/kg sec	i_m	= 10	mA
C	= 0.078	cm^5/kg	ω_n	= 95	rad/sec
D_p	= 19	kg sec/cm	ζ	= 0.7	
P_s	= 18	kg/cm^2	q	= 0.18	

7.2 Experimental results

Though the spiral optimum switching curves are necessary for $\zeta=0.7$ in the actual system, the switching line through the origin is used for simplicity. The position-plus-velocity signal is produced in the analog computer by differentiating the output displacement signal. To avoid the effect of the noise, the dead band was inserted near the zero velocity. When the velocity enters this region, the controller is switched off and the load stops.

Fig. 22 and Fig. 23 show the output displacements and the input voltage to the servo valve for the initial point $x_0=3.95$ mm and $x_0=2.44$ mm, respectively. The controller is switched at point S. The actuating signal is switched off at point L where the load velocity enters the dead band.

Fig. 24 shows the maximum errors for the various initial conditions. They were obtained by twenty experiments under the same condition. The terminal errors were measured by a dial gauge. The maximum errors are less than 0.02 mm.

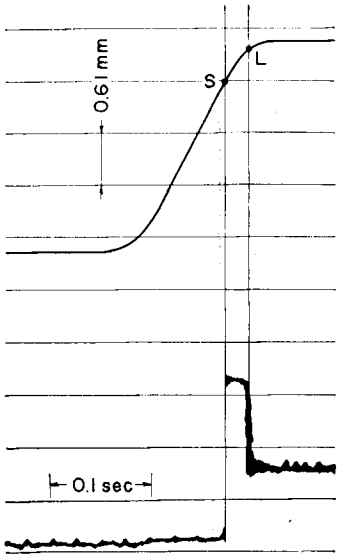

Fig. 22. Output displacement of an actuator and an input voltage to a torquemotor for x_0=2.44 mm and supply pressure=18 kg/cm^2

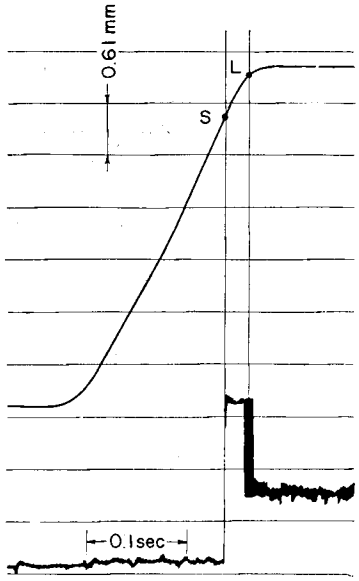

Fig. 23. Output displacement of an actuator and an input voltage to a torquemoter for x_0=3.95 mm and supply pressure=18 kg/cm^2

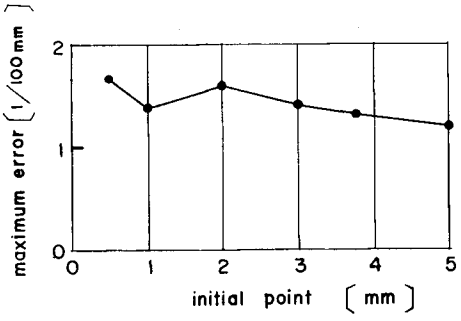

Fig. 24. Relation between maximum errors and initial points

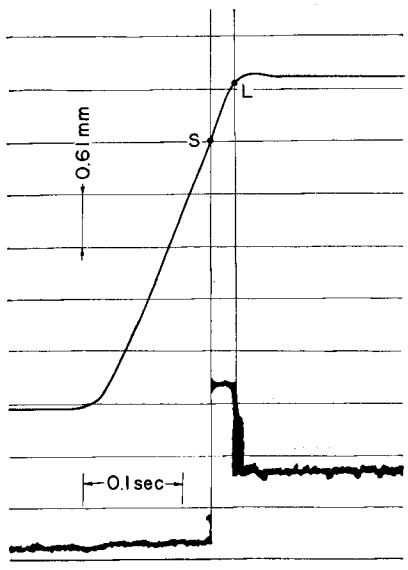

Fig. 25. Output displacement of an actuator and an inut voltage to a torquemotor for x_0=3.88 mm and supply pressure=30 kg/cm^2

Fig. 25 shows the response with the supply pressure 30 kg/cm^2. The table is pulled back after the stop. This is due to the final acceleration over the limit of Eq. (5).

8. Conclusion

For the position control by the valve-controlled electro-hydraulic servomechanisms the optimum control was obtained by the one time switching of the controller and the optimum switching surface was determined. The effect of the magnitude of the control and the friction force to the control accuracy was discussed.

The quasi-optimum controls which are the approximation of the switching curve in the phase plane by the switching lines and of the switching surface in the phase space by the switching plane were presented. The control accuracies were examined for these approximations.

By the experiment, the high control accuracy was obtained and the possibility of the practical use is verified.

Nomenclature

A_p	: effective area of a piston	[cm^2]
D_p	: viscous damping coefficient	[kg sec/cm]
F_s	: static friction force	[kg]
F_v	: kinetic friction force	[kg]
i	: input different current	[mA]
i_m	: rated different current	[mA]
k_1	: flow gain of servo valve	[cm^3/sec mA]
k_2	: flow sensitivity to output pressure	[cm^5/kg sec]
M_p	: mass of the moving parts	[kg sec^2/cm]
T_f	: velocity feedback coefficient	[—]
x	: output displacement	[cm]
A	: initial position	[—]
B	: initial acceleration	[—]
P	: terminal acceleration	[—]
q	: kinetic friction	[—]
T	: control period	[—]
z	: output displacement	[—]
u	: control	[—]
τ	: time	[—]
ζ	: damping coefficient	[—]
ω_n	: natural frequency	[—]

References

1) J.F. Blackburn, G. Reethof and J.L. Shearer: "Fluid Power Control", John Wiley & Sons. (1960)
2) L.S. Pontryagin, V.G. Boltyanskii, R.V. Gamkreliage and E.F. Mishenko: "The Mathematical Theory of Optimal Process", John Wiley & Sons. (1962)
3) R. Tomovic: "Sensitivity Analysis of Dynamic Systems", McGraw-Hill (1964)
4) H. Hanafusa and M. Ikeda: Journal of JAACE. Vol. 12 No. 6 (1968)
5) Y. Sakawa and C. Hayashi: Proc. of 2nd IFAC Theory p. 339 (1963)
6) J.T. Tou: "Modern Control Theory", McGraw-Hill (1964)
7) J. Matsuzaki and M. Hashimoto: Trans. of the JSME. Vol. 28 No. 194 p. 1394 (1962)
8) I. Flugge-Lotz and H.A. Titus: Trans. of the ASME. Ser. D, 5 Basic Eng. p. 554 (1962)
9) I. Flugge-Lotz and H.A. Titus: Proc. of 2nd IFAC Theory, p. 339 (1963)